J. Ocean Univ. China (Oceanic and Coastal Sea Research)
https://doi.org/10.1007/s11802-021-4545-2
ISSN 1672-5182, 2021 20 (2): 372-382
http://www.ouc.edu.cn/xbywb/
E-mail:xbywb@ouc.edu.cn

Corrosion Mechanism of 5083 Aluminum Alloy in Seawater Containing Phosphate

WANG Jiaming[1)], YANG Haodong[1)], DU Min[1), *], HOU Jian[2)], PENG Wenshan[2)], and LIN Cunguo[2), *]

1) *The Key Laboratory of Marine Chemistry Theory and Technology*, *Ministry of Education*, *College of Chemistry and Chemical Engineering*, *Ocean University of China*, *Qingdao* 266100, *China*
2) *State Key Laboratory for Marine Corrosion and Protection*, *Luoyang Ship Material Research Institute (LSMRI)*, *Qingdao* 266237, *China*

(Received March 30, 2020; revised October 21, 2020; accepted October 27, 2020)

Abstract As a material with good corrosion resistance, 5083 aluminum alloy has a great application prospect in marine environment. In this work, the corrosion characteristics of 5083 aluminum alloy in seawater containing phosphate were investigated with Potentiodynamic Polarization, Electrochemical Impedance Spectroscopy (EIS), Scanning Electron Microscope (SEM), Energy Dispersive Spectroscopy Analysis (EDSA), X-ray Photoelectron Spectroscopy (XPS) and Laser Confocal Microscope. The results indicated that the effects of phosphate in seawater were two-fold. Firstly, phosphate slightly accelerated the corrosion of 5083 in seawater in the early stage of corrosion. HPO_4^{2-} competed with OH^- in the adsorption process on the alloy surface, which weakened the contact between OH^- and Al^{3+} near the interface of the alloy, and inhibited the formation as well as the self-repair of the passive film, thus accelerating the activation dissolution process. Compared with the natural seawater, the charge transfer resistance of 5083 in the seawater containing phosphate decreased faster during the early stage of corrosion, and the corrosion current density i_{corr} was higher in seawater containing phosphate. On the other hand, the addition of phosphate would not affect the cluster distribution of the second phase of 5083 in seawater, but it changed the composition of the corrosion product layer and had an obvious inhibitory effect on the local corrosion of 5083 in seawater. After 16-day exposure, shallower and more sparsely distributed pits could be observed on the derusted surface of 5083 in the seawater containing phosphate, and the pitting coefficient in the seawater containing phosphate was significantly lower than that in natural seawater. The reduction of pitting tendency could be realized mainly through two ways. First, the HPO_4^{2-} adsorbed on the surface of the passive film in the early stage of corrosion and repeled the corrosive anions such as Cl^-. Second, phosphate participated in the construction of the $CaHPO_4$ precipitation film, which acted as a barrier and protection.

Key words 5083 aluminum alloy; seawater containing phosphate; pitting corrosion; passive film; Cl^-

1 Introduction

Aluminium alloys are used in a wide range of fields such as aerospace, marine transportation, fast ship, cycling and automobile due to low density, high specific strength, excellent weldability, high corrosion resistance and other functional characteristics (Wagner, 2018). Many excellent properties of aluminum alloys are largely due to their passivation behavior, and researchers have studied the passive film of aluminum alloy from different directions in recent years. Theivaprakasam *et al*. (2018) suggested that the hybrid electrolytes formed by the conventional lithium battery electrolytes and the neat ionic liquids allow an effective and improved passivation of aluminium and lower the extent of aluminium dissolution. Huang *et al*. (2016) proposed that the film formation above the passive film in trihexyl (tetradecyl) phosphonium diphenylphosphate ([P6,6,6,14][dpp]) ionic liquid enhanced the corrosion resistance of AA5083 aluminium alloy. Nam *et al*. (2016) found out that the use of the $Y(4NO_2Cin)_3$ compound made 6061 aluminium alloy more resistant to corrosion in chloride ion media.

5083 aluminum alloy is group with Al-Mg series aluminum alloy, which Mg plays a major strengthening role through solid solution strengthening (Kaoru *et al*., 2001). Bach *et al*. (2019) proposed that Mg and AlN composite addition reduced the grain sizes and defects in the alloy matrix, thus improved pitting resistance of Al-based alloy. Nam *et al*. (2019) suggested that the addition of Mg to Al-based alloy facilitates passive film formation based on the incorporation of Al and Mg oxides/hydroxides, and with the increase of magnesium content, the density and adhesion of the passivation layer on the alloy surface were enhanced. The corrosion of 5-series aluminum alloy

* Corresponding authors. E-mail: ssdm99@ouc.edu.cn
E-mail: lincg@sunrui.net

in seawater showed the characteristics of local corrosion in the early stage and uniform corrosion in the later stage, and the local corrosion is mainly pitting corrosion, crevice corrosion and the intercrystalline corrosion (Natishan *et al*., 2002). 5083 aluminum alloy is a kind of passivating alloy, and its corrosion resistance in seawater environment largely depends on the passive film on its surface. The impurity anion in corrosive mediums can contribute to the corrosion of aluminum alloy (Soltis, 2015), and the strong erodibility of Cl^- and the presence of second-phase metal leads to the pitting corrosion of aluminum alloy in seawater (Jones *et al*., 2001; Jafarzadeh *et al*., 2008; Yang *et al*., 2008).

Inorganic phosphate is a common precipitation film corrosion inhibitor, which is effectively applied to the corrosion protection of iron based materials (Andrade *et al*., 1992; Dhouibi *et al*., 2003; Agnès *et al*., 2005) and copper-based materials (Lytle and Nadagouda, 2010; Yohai *et al*., 2011). As for the effect of phosphate on corrosion of aluminum alloy in corrosive medium, Rudd and Scully (1980) proposed that phosphate had the effect of inhibiting pitting corrosion of aluminum alloy, Wang *et al*. (2000) believed that the hydrolysis of phosphate promoted the formation of $Al(OH)_3$ precipitation membrane by offering more OH^-. In general, there are several theories about the mechanism of the effect of phosphate on the corrosion of aluminum alloy, such as the pH effect, the formation of insoluble precipitation film, and the occupation of active sites of anode and cathode. Seawater is a natural buffer so the pH effect is limited, and the presence of calcium ions in seawater limits the upper limit of the concentration of phosphate. In this paper, phosphate is regarded as the nutrient pollutant in the seawater, and the effect of the phosphate on the corrosion of 5083 in the seawater is studied.

2 Experiment

2.1 Materials and Solutions

The electrode material used in the experiment was 5083 aluminum alloy made in China, and its chemical composition content is shown in the table below:

Table 1 Chemical composition content of 5083 aluminum alloy (wt%)

Element	Si	Cu	Mg	Zn	Mn	Ti	Cr	Fe	Al
Content	≤0.4	≤0.1	4.0–5.0	≤0.25	0.4–1.0	≤0.15	0.05–0.25	≤0.4	Remaining

The specimens used for electrochemical measurements had a dimension of 10 mm × 10 mm × 3 mm, leaving a working area of 1 cm^2. The work face of the specimens was abraded with 600, 800 and 1200-grit silicon carbide metallurgical papers sequentially, degreased by anhydrous ethanol, and was then dried in the air for 24 h.

The seawater was taken from the sea area of Shazikou, Qingdao, Shandong. The temperature of the corrosive medium was kept at 25℃±0.2℃, and the initial pH was 7.9±0.1. In what's called 'seawater containing phosphate', the concentration of phosphate was increased to 0.025 mmol L^{-1} by adding analysis pure $Na_2HPO_4{\cdot}12H_2O$. The total concentration of phosphate was increased to 0.025 mmol L^{-1}. The value was selected based on the order of magnitude of the concentration of Ca^{2+} (0.5–1.0 μmol L^{-1}) in natural seawater and the Ksp (2.0×10^{-29}, 20℃) of calcium phosphate, and a high value was selected on the premise of no precipitation.

2.2 Electrochemical Measurements

All the electrochemical measurements were performed using a Gamry potentiostat (Reference 600) with a saturated calomel electrode (SCE) as the reference electrode and platinum plate as the counter electrode. Electrochemical impedance spectroscopy (EIS) was tested at the steady-state open circuit potential (OCP) by applying a sinusoidal voltage signal of 10 mV in the frequency range of 10^5–10^{-2} Hz. The EIS data were analyzed using Zview2 software (Scribner Inc.) with a suitable equivalent circuit model.

Potentiodynamic polarization curves were measured by scanning the potential from OCP to +300 mV versus OCP at a sweep rate of 1 mV s^{-1}.

And the polarization curves were analyzed using Cview 2 software (Scribner Inc.). All experiments were carried out at 25℃ in airtight system and repeated at least three times.

2.3 Surface Analysis

Scanning electron microscope (Tescan Vega 3, Czech Republic) was used to observe the morphology of the corrosion product (SEM HV=20 kV). The energy dispersive X-ray spectrometer (EDS) was used to analyze the element composition and distribution of corrosion product, the EDS surface scanning lasted for 5 min for each specimen. X-ray photoelectron spectroscopy (XPS, Themo-Scientific Escalab 250Xi, USA) was used to analyze the composition of corrosion products on the specimen surfaces utilizing monochromatic Al Kα radiation. Laser confocal microscope (KEYENCE vk-250) was used to observe the local corrosion behavior of the derusting substrate, which was soaked in 0.5 mol L^{-1} nitric acid for 5 min to derust the surface.

3 Results and Discussion

3.1 Open Circuit Potential

Fig.1 showed the variations of the open circuit potential (*vs*. SCE) of 5083 aluminum alloy in seawater with time. The OCP of 5083 aluminum alloy showed a general trend of fluctuation and decline in both natural seawater and seawater containing phosphate, and it varied from −750 mV to −820 mV (*vs* SCE). The difference lied in the significant positive shift of OCP in the middle stage of

corrosion (the 9th day) in the seawater containing phosphate. The decrease of OCP may be due to the formation of corrosion product film, which obstructed the diffusion of dissolved oxygen in the medium to the electrode surface, thus inhibiting the cathode depolarization reaction on the electrode surface (Liu *et al*., 2016). The different changes of OCP suggested that the presence of high concentration of phosphate influenced the electrochemical corrosion process of 5083 in seawater.

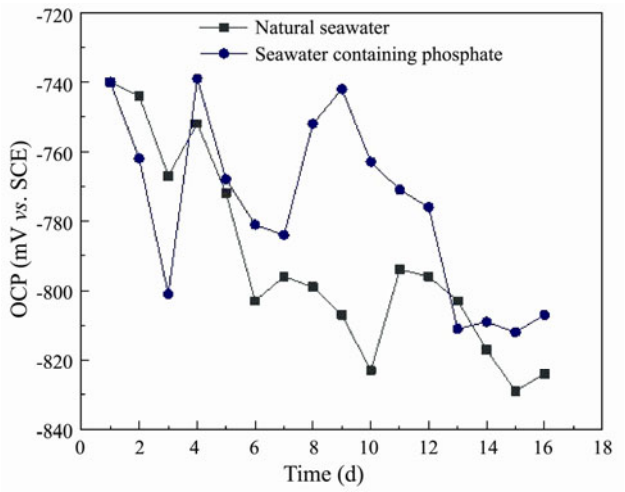

Fig.1 Open circuit potential (*vs* SCE) of 5083 aluminum alloy in seawater.

3.2 Electrochemical Impedance Spectroscopies

Electrochemical impedance spectroscopies (EIS) was used to evaluate the corrosion electrochemical characteristics of the interfaces. Fig.2, depicted the EIS of the 5083 aluminium alloy in seawater in the forms of Nyquist and Bode plots. Based on the shape and surface analysis of EIS graph, the equivalent circuit shown in Fig.3 was obtained, and the fitting data obtained from the equivalent circuit was shown in Table 2. In Fig.3, R_s referred to Solution Resistance, R_{ct} referred to Charge Transfer Resistance, CPE refered to the Phase Angle Elements which consisted of the Faraday Capacitance-C_{dl} and the dispersion coefficient of electrochemical reaction n_d.

During the first 7 d of its immersion, impedance of 5083 decreased along with immersion time in both natural seawater and seawater containing phosphate, indicating the destruction and weakening of passive film formed on alloy surfaces. The change trend of capacitive reactance radius and the change of R_{ct} indicated that the corrosion process of 5083 accelerated in the first seven days and decreased after that. Compared to the natural seawater, the decline of R_{ct} in the seawater containing phosphate had been faster and greater. The value of n_{dl} reflects the integrity of the interface film between the alloy and the medium, the closer n_{dl} is to 1, the more integrated the film is. The Fig.4 suggested that the variation of n_{dl} showed same regularity in both medium, which declined

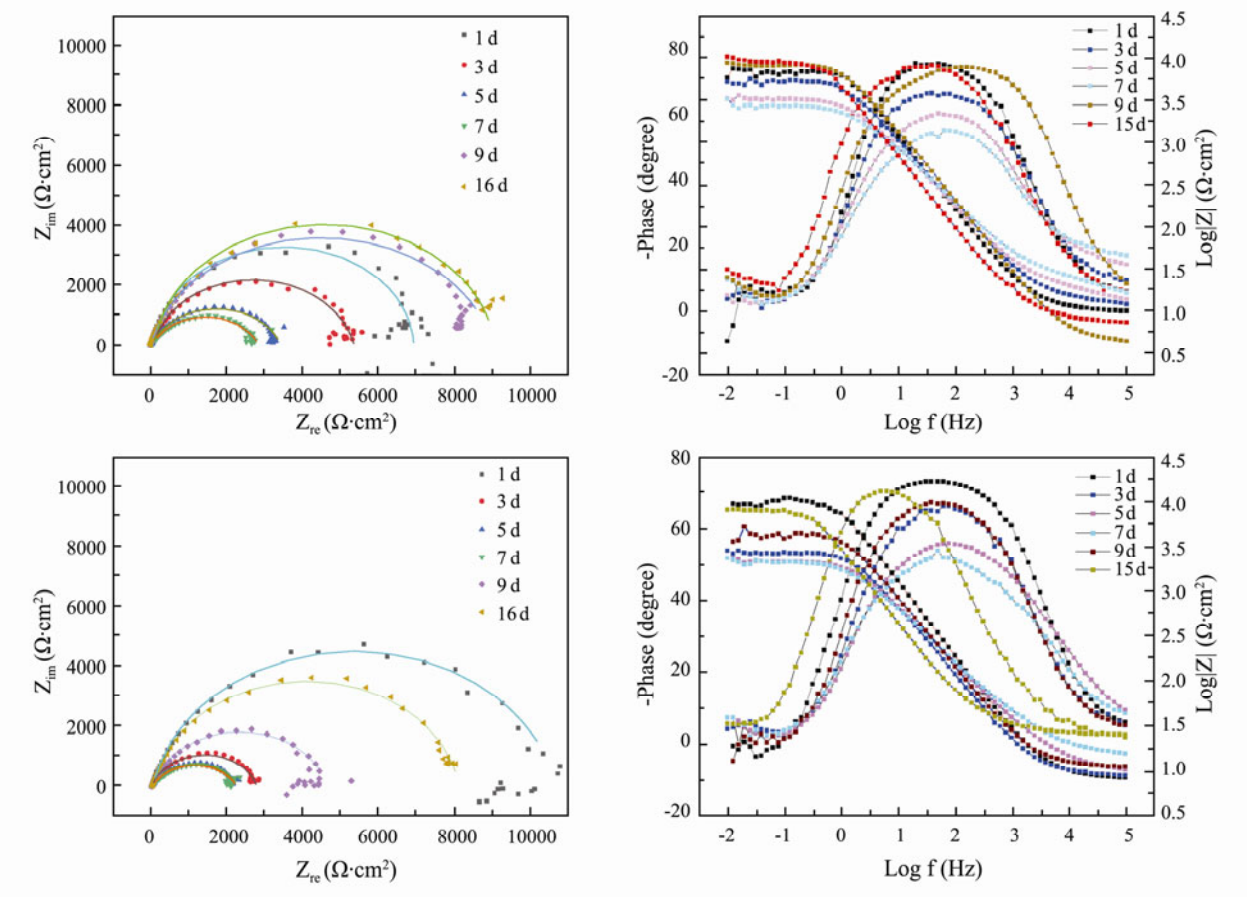

Fig.2 Electrochemical impedance spectrum of 5083 in seawater.

Table 2 The fitting data of EIS of 5083 aluminum alloy in seawater

Medium	Time (d)	R_s ($\Omega\,cm^2$)	C_{dl1} ($\mu F\,cm^{-2}$)	n_{d1} (/)	R_f ($\Omega\,cm^2$)	C_{dl2} ($\mu F\,cm^{-2}$)	n_{d2} (/)	R_{ct} ($\Omega\,cm^2$)
Natural seawater	1	10.33	25.4	0.8538	88430	17.1	0.9359	6785
	3	12.45	39.4	0.76996	75022	24.4	0.8703	5291
	5	15.21	68.4	0.69461	52501	41.8	0.7758	3416
	7	16.50	101.7	0.61794	49270	48.5	0.7454	2801
	9	4.534	19.5	0.85540	97402	20.3	0.8547	9006
	16	7.859	47.8	0.87420	87994	31.9	0.9319	8957
Seawater containing phosphate	1	8.421	24.2	0.83605	92650	18.2	0.8940	10638
	3	8.974	50.8	0.79367	48174	41.7	0.8364	2770
	5	9.459	76.5	0.64943	31325	53.2	0.7650	2223
	7	14.46	123.7	0.61259	32543	66.4	0.7231	2211
	9	11.13	41.6	0.79478	67980	32.1	0.8530	4621
	16	26.57	10.12	0.76885	75432	22.4	0.9145	8046

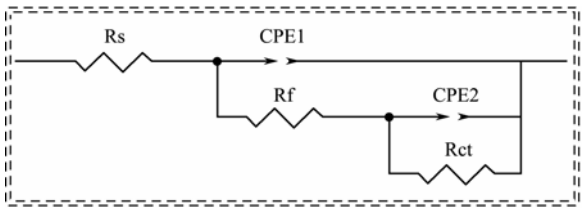

Fig.3 Physical model for simulating an equivalent circuit to fit the EIS data.

in the first 7 d and rose later. This indicated that the surface integrity of the passive film decreased first and then increased in both medium. This indicated that the destructive effect of corrosive ions such as Cl^- in the early corrosion stage was dominant, while the self-repair of passive film and the protection of corrosion products in the late corrosion stage were dominant. Meanwhile, the n_{d1} in the seawater containing phosphate was slightly less than that in the natural seawater, which suggested that the quality of the passive film was worse in the seawater containing phosphate. Conde and De Damborenea (2006) pointed out that the appearance of the contain arc in the low-frequency region was related to the adsorption of Cl^-, Cao *et al*. (2008) suggested that when chloride ions were adsorbed on the surface of the passive film and the dissolution rate of the local passive film was higher than the self-repair of the film, the inductive arc resistance could be observed in the low frequency region of the impedance spectrum. During the pit initiation of the pitting corrosion of passivated metal, the low-frequency inductive arc in the impedance spectrum shrank with time, and when the passivated film was dissolved through, the low-frequency inductive arc in the impedance spectrum also disappeare (Jafarzadeh *et al*., 2008). As shown in the Nyquist plots of Fig.2, the inductive arc of the natural seawater was obvious on the first day and the features of it became less apparent over time, it disappeared on the fifth day and had been displaced by Warburg impedance lately, which suggested that the passive film of 5083 in the natural seawater had been brokethrough by the corrosive ion during the early stage of the corrosion. In the seawater containing phosphate, the contain arc shrank with time as well, but no Warburg impedance could be observed, which meant that ion adsorption of corrosive Cl^- occurred on the surface of the alloy but the passive film had not been brokethrough ultimately.

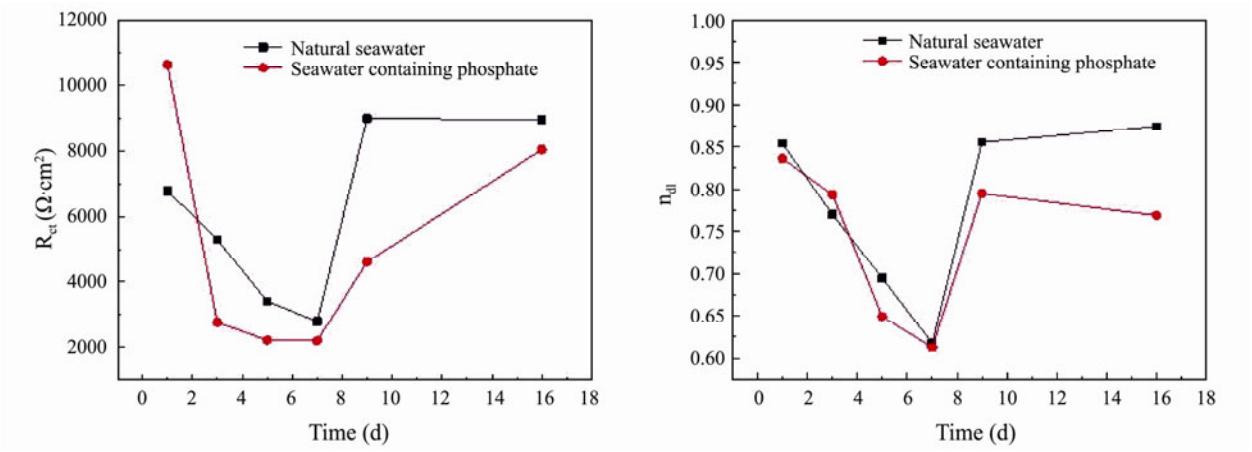

Fig.4 The changing trend of R_{ct} and n_{d1}.

3.3 Anodic Polarization Curves

Fig.5 showed the potentiodynamic polarization curves of 5083 after 1 and 16 d exposed in the natural seawater and the seawater containing phosphate. The measured polarization curves were fitted through Cview2 software to obtain electrochemical parameters, the linear fitting method of strong polarization region (>70 mV) was ado-

pted in the fitting, the fitting data were listed in Table 3, *e.g.*, anode Tafel slope (b_a), self-corrosion current density (i_{corr}), corrosion potential (E_{corr}), pitting potential (E_{pit}). The anode polarization diagram of 5083 in the natural seawater showed obvious characteristics of passivation and breakthrough of the passive film. Epit of 16d in the natural seawater was higher than that of 1d, which suggested that with the development of corrosion product film, the pitting resistance of the alloy surface was gradually improved. The i_{corr} in the seawater containing phosphate was slightly smaller than that in the natural seawater when soaked for the same time, and the i_{corr} of 16 d was higher than that of 1 d, which could be explained by the decline of the densification and surface of the passive film. The b_a of 1 d in the seawater containing phosphate was obviously smaller than that in the natural seawater, but the values of the b_a of 16 d were similar in two mediums, which indicated that the promoting effect of phosphate on the activation dissolution process mainly occurred in the initial stage of corrosion.

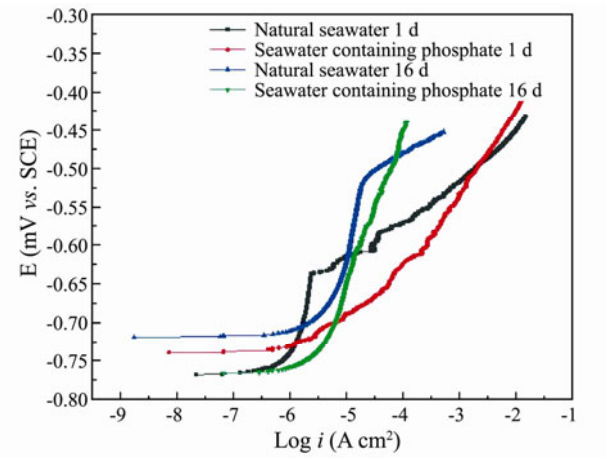

Fig.5 Anodic polarization curves of 5083 in seawater.

Table 3 The fitting data of POT of 5083 aluminum alloy in seawater

Medium	Time (d)	b_a (mV dec^{-1})	i_{corr} (μA cm^{-2})	E_{corr} (V)	E_{pit} (V)
Natural seawater	1	307.15	1.23	−0.776	−0.635
	16	219.24	2.29	−0.721	−0.509
Seawater containing phosphate	1	153.27	1.29	−0.740	-
	16	198.31	2.45	−0.768	-

3.4 Morphology Characterization and Component Analysis of Corrosion Product

The morphologies of corrosion product were characterized by Scanning Electron Microscope (SEM). Fig.6 showed surface morphologies of 5083 aluminum alloy after exposure to natural seawater, seawater containing phosphate for 4 and 16 days. It could be seen from the SEM image, that the morphology of the corrosion product of 5083 was similar in natural seawater and seawater containing phosphate, after immersed for four days. Corrosion product had started to generate on the surface of the material, but the amount was not enough to cover the whole surface, and the scratches on the substrate were clearly visible. In addition, the uniformity of the surface of the alloy got worse than the original state, and metallic inclusion in the second phase could be obviously observed (as shown in the A area of Fig.6).

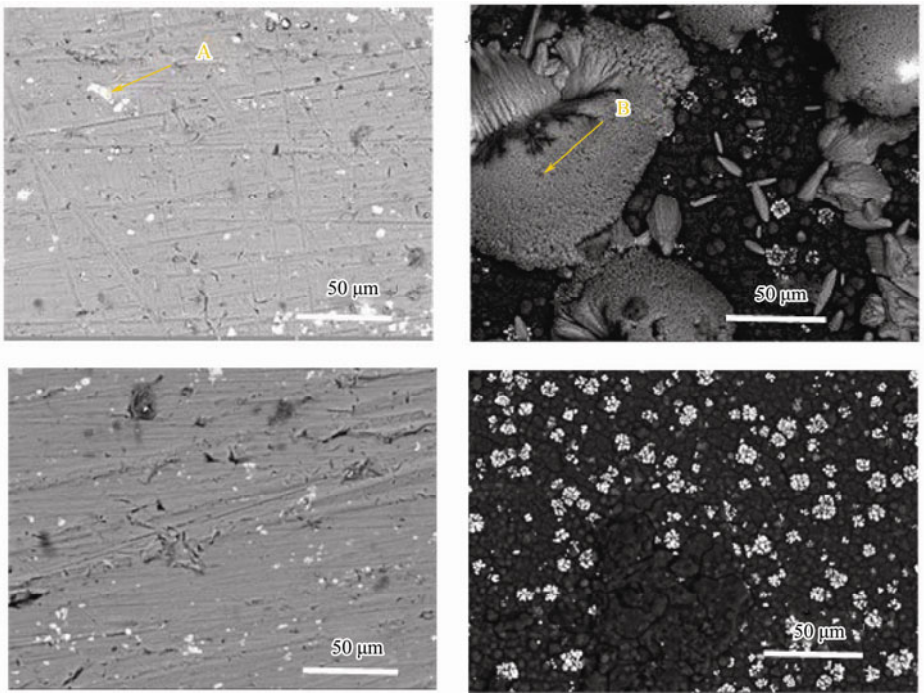

Fig.6 Scanning electron micrograph of corrosion product of 5083 aluminum alloy in seawater. a, natural seawater 4 d; b, natural seawater 16 d; c, seawater containing phosphate 4 d; d, seawater containing phosphate 16 d.

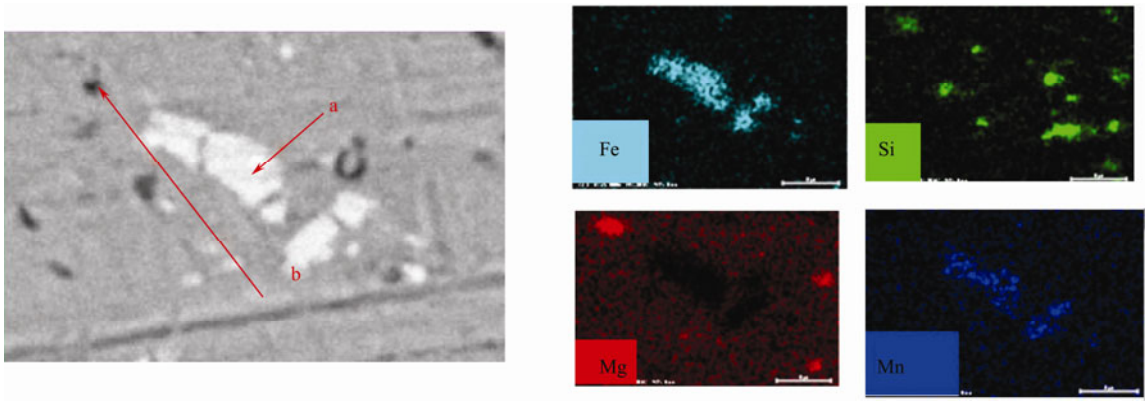

Fig.7 Distribution diagram of element of corrosion product of the 5083 aluminum alloy in natural seawater for 4 d.

After immersed for 16 days, the corrosion product had covered the whole surface of the material and could be divided into two parts: a dense layer of corrosion product next to the metal base and other components deposited on it. $CaCO_3$ precipitate (as proved in Fig.7) could be observed in the natural seawater (as shown in the B area of Fig.6), but could not be observed in the seawater containing phosphate.

EDS was used to analyze the element composition and distribution of corrosion product. The EDS surface scanning results showed that the composition of corrosion product was similar in natural seawater and seawater containing phosphate after four-day exposure. Fig.8 showed the distribution of elements of corrosion product of the 5083 aluminum alloy in natural seawater for 4 d, there was cluster distribution of Mn-Fe on the corrosion product, which reflected the second phase of 5083 alloy. The 'a' area of Fig.6 corresponded to the Al-Fe-Mn phase, which was consistent with the results obtained by Jaya *et al*. (2018). The 'b' area of Fig.8 corresponded to the Mg_2Si phase, which was consistent with the results obtained by Jones *et al*. (2001). In addition, parts of Si may exist in the form of SiO_2 (Huang *et al*., 2016).

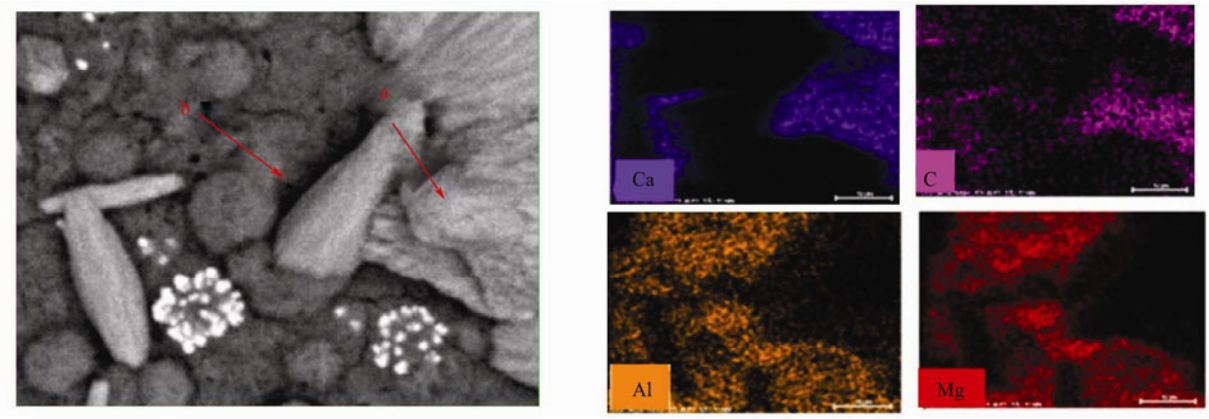

Fig.8 Distribution diagram of element of corrosion product of the 5083 aluminum alloy in natural seawater for 16 d.

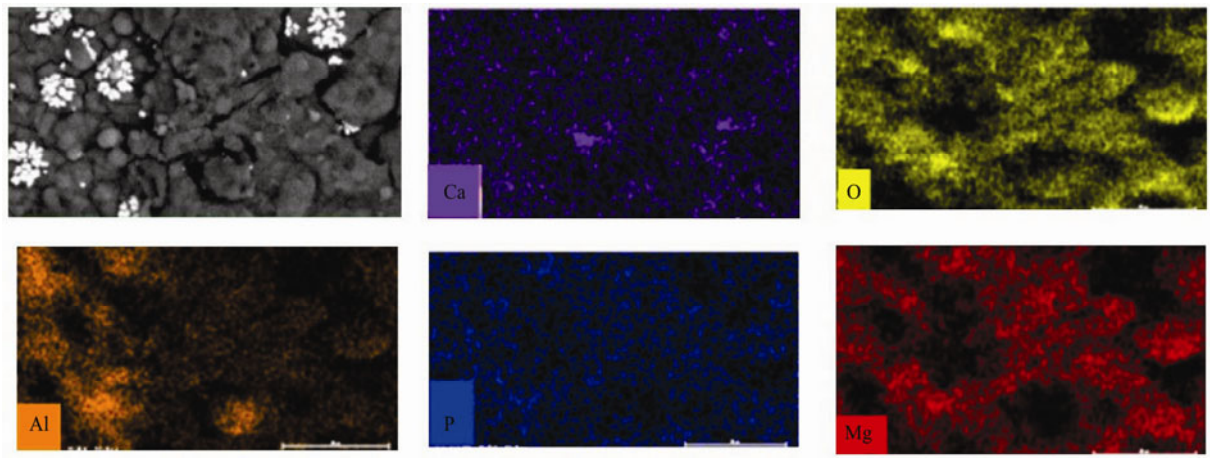

Fig.9 Distribution diagram of element of corrosion product of the 5083 aluminum alloy in seawater containing phosphate for 16 d.

Fig.9 showed the EDS surface scanning results of the corrosion product of the 5083 aluminum alloy in the seawater containing phosphate, which revealed that Ca and P were uniformly distributed among the corrosion product, and their existence had been proved to be in the form of $CaHPO_4$ by the means of XPS (as shown in Fig.10). Table 4 showed the atomic ratio of Ca and P of corrosion product of 5083 aluminum alloy in the seawater containing phosphate by EDS, it could be seen that the atomic ratio of Ca and P increased with time, which reflected the process that $CaHPO_4$ gradually covered the alloy surface to form a precipitation coating.

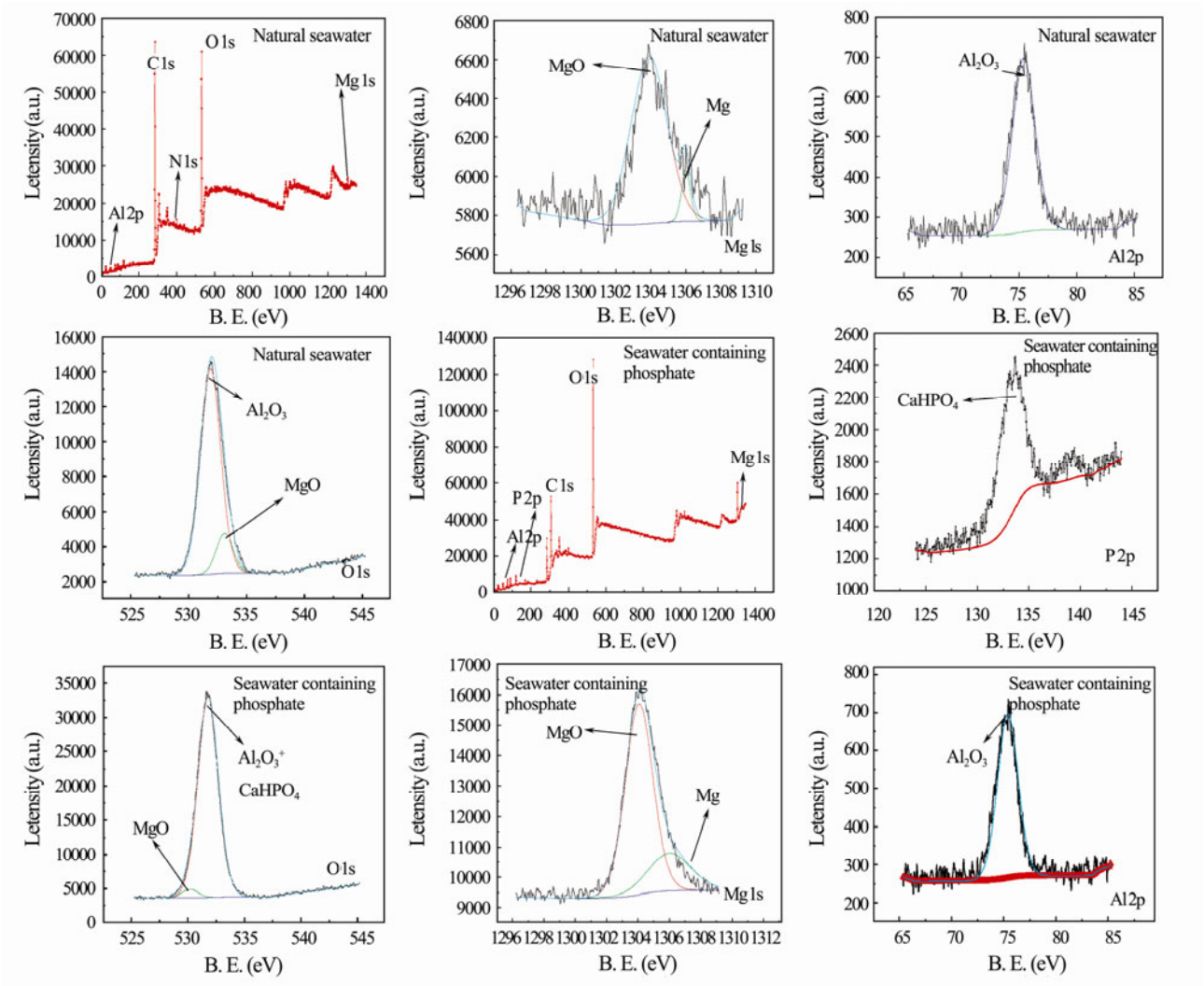

Fig.10 XPS spectrum of corrosion product of 5083 aluminum alloy immersed in seawater for 16 d.

Table 4 Atomic ratio of Ca and P of corrosion product of 5083 aluminum alloy in the seawater containing phosphate by EDS

Time (d)	Atomic ratio (%)	
	Ca	P
4	0.09	0.14
8	0.18	0.27
16	0.61	0.72

3.5 Evaluation of Pitting Corrosion by Laser Scanning Confocal Microscope

Laser confocal microscope and optical profilometry were used to evaluate the severity of the pitting corrosion of 5083, and 3D models of the derusting substrate were established as shown in Fig.11. It could be indicated from Fig.11 that the corrosion pits were deeper and more concentrated in the natural seawater. Fig.12 showed the distribution diagram of pits deeper than 5 μm after 16 d exposure in natural seawater and seawater containing phosphate. Fig.12 suggested that pits deeper than 5 μm spread wider in the natural seawater than in the seawater containing phosphate. Fig.11 and Fig.12 intuitively supported the fact that the pitting tendency of 5083 was significantly reduced when phosphate was added in the seawater.

Quantitative fitting data of pitting corrosion of 5083 in seawater for 16 d were shown in Table 5 and the quantitative treatment of pitting data were carried out according to the formula (3.5-1) and (3.5-2). The results showed that the average depth of pits of 5083 in the natural seawater for 16 d was 2.8 μm, the pitting circle equivalent diameter was 34.3 μm, and the pitting coefficient was 18.57. The equivalent diameter was much larger than the

average pitting depth, which indicated that the self-passivation of aluminum alloy hindered the longitudinal development of the pitting corrosion, and the corrosive ions had difficulties going deeper.

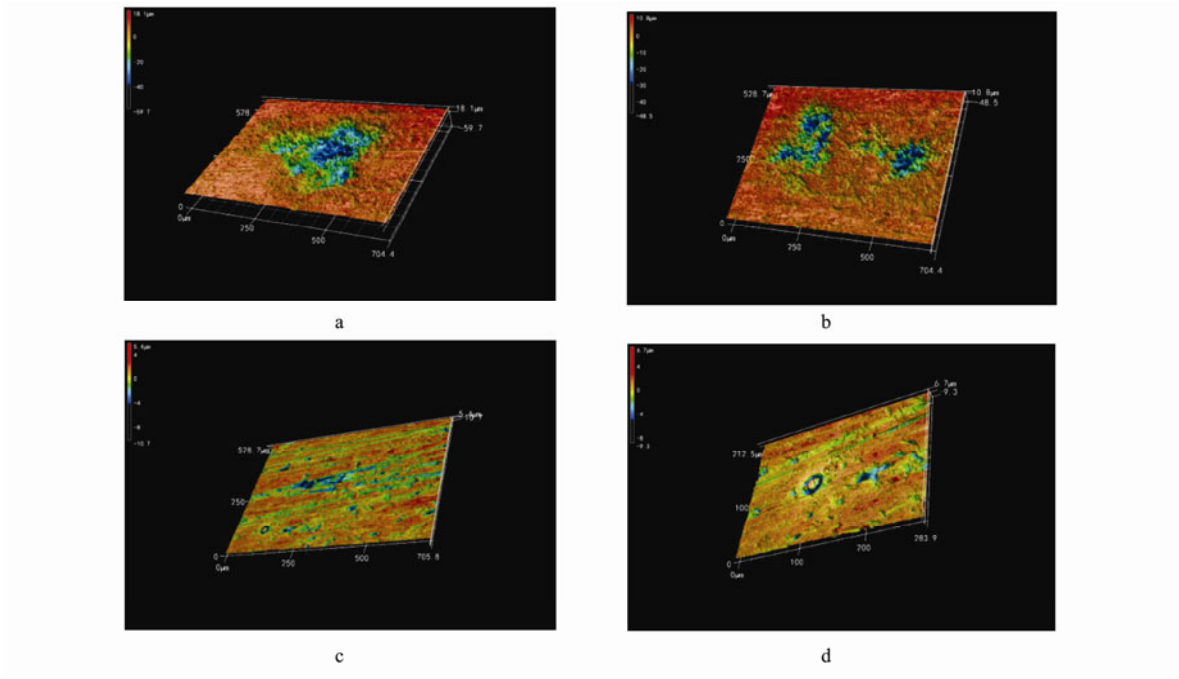

Fig.11 3D model of the derusting substrate surface of 5083 in seawater for 16 d. a and b, natural seawater; c and d, seawater containing phosphate.

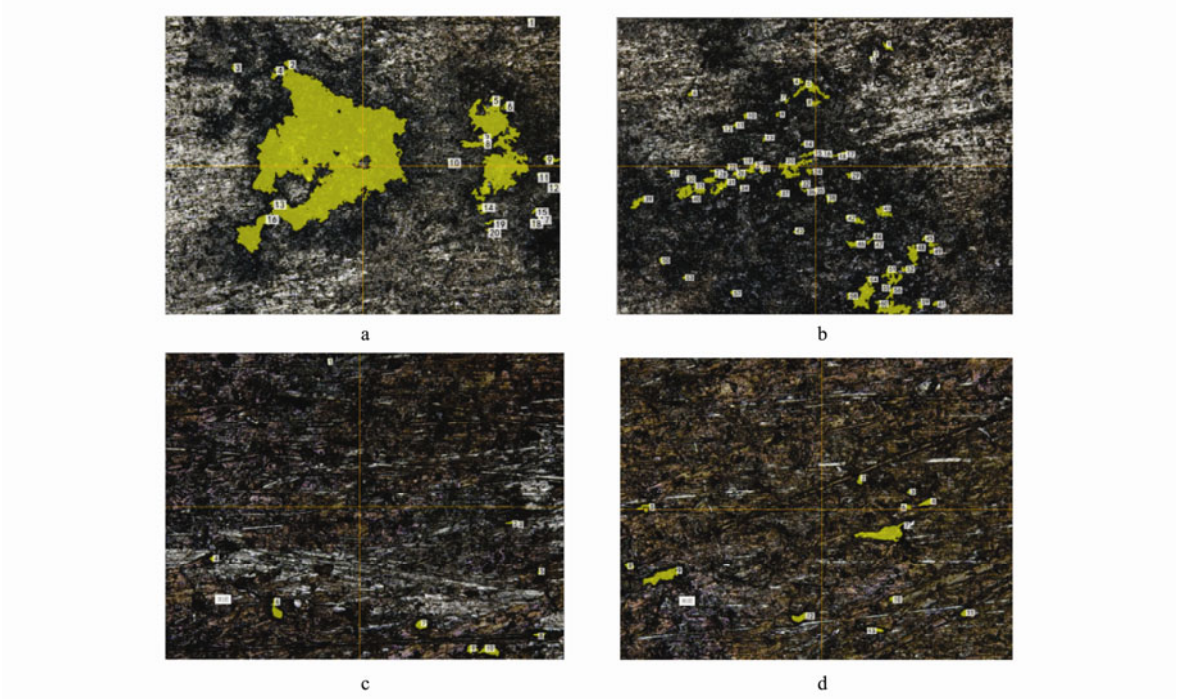

Fig.12 Distribution diagram of pits deeper than 5 μm of 5083 in seawater for 16 d. a and b, natural seawater; c and d, seawater containing phosphate.

Table 5 Quantitative fitting data of pitting corrosion of 5083 in seawater for 16 d

Medium	Number of pits deeper than 5 ($\mu m\,cm^{-2}$)	Average depth of pits (μm)	Pitting circle equivalent diameter (μm)
Natural seawater	1868	−2.8	34.3
seawater containing phosphate	2951	−1.2	14.5

In the seawater containing phosphate, the average depth of pits was 1.1 μm which was shallower than in the natural seawater, the pitting circle equivalent diameter was 14.5 μm which is smaller than in the natural seawater,

and the pitting coefficient was 7.16 which is lower than in the natural seawater, which mean that there were lower pitting coefficient and lower regional average pit depth in the seawater containing phosphate.

The fitting data and the diagrams echoed each other, supporting the claim that the added phosphate reduced the pitting tendency of 5083 in the seawater. In addition, the lower pitting density in the natural seawater could be explained by the formation of large pits formed by the joint of small pits.

The obtained data were processed according to the following formula:

$$P_{\text{pit}} = \frac{N}{S}, \tag{3.5-1}$$

$$A = \frac{h_{\max}}{h_{\text{ave}}}. \tag{3.5-2}$$

P_{pit}: mean pitting density (cm^{-2})
N: number of pits in the region
S: area (cm^2)
A: pitting coefficient
$h_{\max}$: depth of the deepest pit (μm)
h_{ave}: average depth of the pits in the region (μm)

3.6 Corrosion Mechanism Discussion

3.6.1 Corrosion mechanism of 5083 in the natural seawater

Fig.13 illustrated the basic corrosion process of 5083 in the natural seawater.

The process (Fig.13a) reflected the main cathodic depolarization reaction occurring in the system: the depolarization reaction of oxygen, which mainly provided OH^- for self-passivation of 5083.

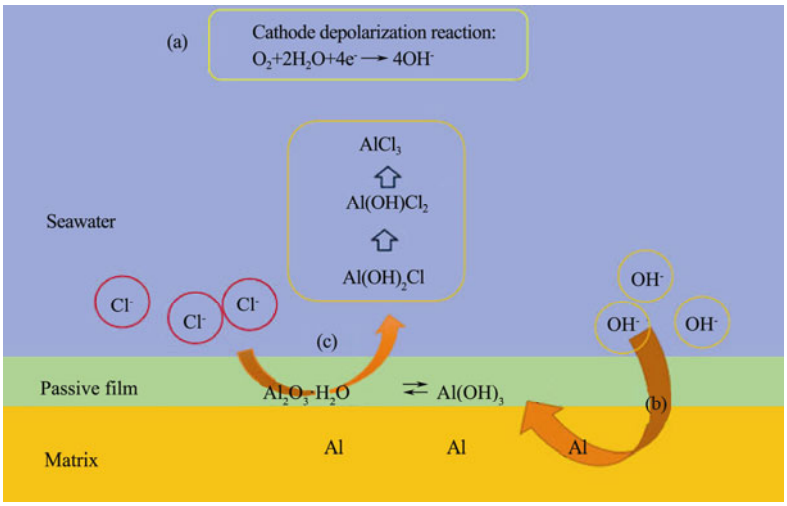

Fig.13 Schematic diagram of corrosion mechanism of 5083 aluminum alloy in natural seawater.

The process (Fig.13b) reflected the self-passivation process of 5083, which could mainly be divided into two steps (3.6-1) and (3.6-2) (Jaya *et al*., 2018). The $Al(OH)_3$ formed in step (3.6-1) was gelatinous, which had poor protective property; while the $Al_2O_3{\cdot}H_2O$ formed in step (3.6-2) was more compact and had better protective property (Zaid *et al*., 2008).

$$Al+3OH^- \rightarrow Al(OH)_3+3e^-, \tag{3.6-1}$$

$$2Al(OH)_3 \rightarrow Al_2O_3{\cdot}H_2O+2H_2O. \tag{3.6-2}$$

Foroulis and Thubricar (1975) suggested that breakdown of the passive film of aluminum alloy by Cl^- occurs in two steps (as shown in the process (c) of Fig.13). Firstly, Cl^- ions adsorbed on the hydrated oxide surface under the influence of the electric field in competition with OH^- or water molecule and then form a soluble, basic chloride salt with the lattice cation.

It is suggested that Cl^- contributed to the conversion of $Al(OH)_3$ into soluble $AlCl_3$ complex through a two-step intermediate process by step-by-step substitution (Conde and De Damborenea, 1997; Zazi and Chopart, 2017) (as shown in the (3.6-3), (3.6-4) and (3.6-5)), so as to lead to the damage even the breakdown of the passive film of the alloy.

$$Al(OH)_3+Cl^- \rightarrow Al(OH)_2Cl+OH^-, \tag{3.6-3}$$

$$Al(OH)_2Cl+Cl^- \rightarrow Al(OH)Cl_2+OH^-, \tag{3.6-4}$$

$$Al(OH)Cl_2+Cl^- \rightarrow AlCl_3+OH^-. \tag{3.6-5}$$

3.6.2 The influence of phosphate added in the seawater

Seawater is a natural buffering system. Under the pH condition of seawater, 90% of the phosphate group exists in the form of HPO_4^{2-}, and adding 0.025 mmol L^{-1} phosphate has little effect on the pH of seawater. Therefore, the inhibition to the pitting corrosion brought by phosphate in seawater is not through the pH effect.

The influence of phosphate in the seawater on the corrosion of 5083 aluminum alloy varied with time and could be divided into three stages as shown in Fig.14.

In the original state (Fig.14a), due to the process of activation dissolution and the presence of positively charged oxygen vacancies (Jafarzadeh *et al*., 2007), there was an

anion-selective outer on the surface of the alloy. Meanwhile, competitive adsorption of anions such as OH^-, Cl^- and HPO_4^{2-} *etc*., happened on the surface of the alloy.

In the early stage of the corrosion (Fig.14b), according to the adsorption model based on the so-called 'bipolar passive film' (Sakashita, 1977), the adsorption and incorporation of HPO_4^{2-} led to the conversion of the anion-selective outer passive film of 5083 into cation-selective phases. Such cation-selective phases might repel Cl^- from the surface and hinder the penetration of the aggressive anions into the passive film, which contributed to inhibit the pitting corrosion. On the other hand, the absorption of OH^- was also hindered by this repulsive interaction, so the self-passivation process of the 5083 alloy was also inhibited and this effect also accelerated the activation and dissolution of the alloy.

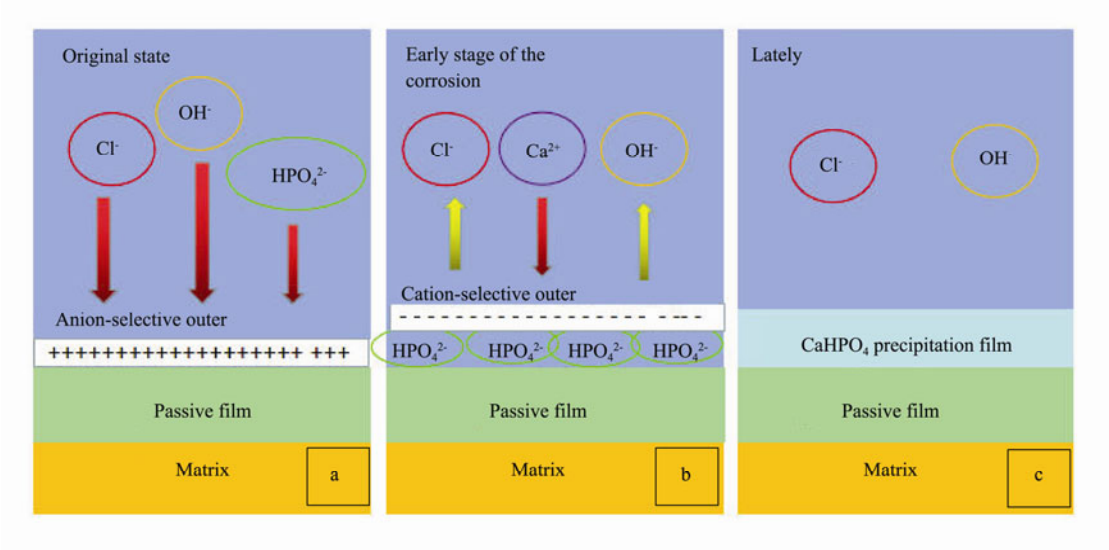

Fig.14 Schematic diagram of the influence of high concentration of phosphate in the seawater on the corrosion of 5083 aluminum alloy.

Basame and White (2000) suggested that addition of anions would contaminate the passive film components and lead to higher conductivity on the permeation path, and the whole process was an autocatalytic acceleration process, which might explain why the results of electrochemical impedance spectroscopy showed that the corrosion rate of 5083 in seawater containing phosphate was slightly higher than that in natural seawater during the early stage of the corrosion.

Lately (Fig.14c), Ca^{2+} in the medium gradually combined with HPO_4^{2-} absorbed on the surface to form $CaHPO_4$ precipitation (as shown in the process (3.6-6)), and with the accumulation of the precipitation, a dense precipitation film gradually formed, which covered the surface of the alloy and acted as a barrier and protection. It could be speculated that with the gradual perfection of precipitation film, the corrosion resistance of the alloy in seawater containing phosphate will gradually improve.

$$Ca^{2+}+HPO_4^{2-}\rightarrow CaHPO_4\downarrow . \quad (3.6\text{-}6)$$

4 Conclusions

High concentration of phosphate in the seawater negatively affected the corrosion resistance of 5083 by inhibiting the self-passivation of 5083 in the early stage of corrosion.

High concentration of phosphate decreased the pitting tendency of 5083 in seawater by inhibiting the adsorption of corrosive ions such as Cl^- and forming a $CaHPO_4$ precipitation barrier film which had good blocking effect. Besides, with the passage of corrosion time, the barrier film was gradually improved to give better protection.

In the seawater containing phosphate, most of Ca element is paticipated in the formation of the $CaHPO_4$ precipitation barrier film on the surface of 5083, which meant that there was much less calcium carbonate deposited on the surface of the corrosion products.

Acknowledgement

This work was supported by the National Natural Science Foundation of China (No. U1706221).

References

Agnès, D. P., William, P., Theophil, L., and Ginette, A., 2005. Detection or quantitative analysis of a corrosion inhibitor, the sodium monofluorophosphate, in concrete. *Cement and Concrete Composites*, **27** (6): 679-687, DOI: 10.1016/j.cemconcomp.2004.11.002.

Andrade, C., Alonso, C., Acha, M., and Malric, B., 1992. Preliminary testing of Na_2PO_3F as a curative corrosion inhibitor for steel reinforcements in concrete. *Cement and Concrete Research*, **22** (5): 869-881.

Bach, L. X., Son, D. L., Phong, M. T., Thang, L. V., Bian, M. Z., and Nam, N. D., 2019. A study on Mg and ALN composite in microstructural and electrochemical characterizations of extruded aluminum alloy. *Composites Part B Engineering*, **156**: 332-343, DOI: 10.1016/j.compositesb.2018.08.139.

Basame, S. B., and White, H. S., 2000. Pitting corrosion of titanium: The relationship between pitting potential and competitive anion adsorption at the oxide fifilm/electrolyte interface.

Journal of the Electrochemical Society, **147** (4): 1376-1381.

Conde, A., and De Damborenea, J., 1996. Effect of surface depletion of lithium on corrosion behaviour of aluminium alloy 8090 in a marine atmosphere. *Journal of Materials Science*, **31**: 4921-4926, DOI: 10.1007/BF00355881.

Conde, A., and De Damborenea, J., 1997. An electrochemical impedance study of a natural aged Al-Cu-Mg alloy in NaCl. *Corrosion Science*, **39** (2): 295-303, DOI: 10.1016/S0010-938X(97)83348-3.

Conde, A., De Damborenea, J., Durán, A., and Menning, M., 2006. Protective properties of a sol-gel coating on zinc coated steel. *Journal of Sol-Gel Science and Technology*, **37** (1): 79-85, DOI: 10.1007/s10971-005-5357-3.

Dhouibi, L., Triki, E., Salta, M., Rodrigues, P., and Raharinaivo, A., 2003. Studies on corrosion inhibition of steel reinforcement by phosphate and nitrite. *Materials and Structures*, **36** (8): 530- 540.

Huang, P., Somers, A., Howlett, P. C., and Forsyth, M., 2016. Film formation in trihexyl(tetradecyl)phosphonium diphenylphosphate ([P6,6,6,14][dpp]) ionic liquid on AA5083 aluminium alloy. *Surface & Coatings Technology*, **303**: 385-395, DOI: 10.1016/j.surfcoat.2015.12.060.

Jafarzadeh, K., Shahrabi, T., and Hosseini, M. G., 2008. EIS study on pitting corrosion of AA5083-H321 aluminum-magnesium alloy in stagnant 3.5% NaCl solution. *Journal of Materials Science and Technology*, **24** (2): 215-219.

Jafarzadeh, K., Shahrabi, T., Hadavi, S. M. M., and Hosseini, M. G., 2007. Role of chloride ion and dissolved oxygen in electrochemical corrosion of AA5083-H321 aluminum-magnesium alloy in NaCl solutions under flow conditions. *Journal of Materials Science and Technology*, **23** (5): 623-628.

Jaya, P. V., Rao, N. M., Kamaluddin, S., and Surya, K., 2018. A study of microstructure and tribological properties of Al 5083 MMC processed by direct extrusion. *Materials Today: Proceedings*, **5** (2): 8232-8240.

Jones, R. H., Baer, D. R., Danielson, M. J., and Vetrano, J. S., 2001. Role of Mg in the stress corrosion cracking of an Al-Mg alloy. *A, Physical Metallurgy and Materials Science*, **32** (7): 1699-1711, DOI: 10.1007/s11661-001-0148-0.

Kaoru, M., Anders, N., and Ingemar, O., 2001. Surface reactions during pickling of an aluminium-magnesium-silicon alloy in phosphoric acid. *Corrosion Science*, **43** (2): 381-396, DOI: 10.1016/S0010-938X(00)00069-X.

Liu, H. X., Du, Q. L., Duan, J. Z., Zhai, X. F., and Hou, B. R., 2016. Effects of natural seawater microorganisms on initial corrosion behavior of 5083 aluminum alloy. *Corrosion Science and Protection Technology*, **28** (1): 51-57.

Lytle, D. A., and Nadagouda, M. N., 2010. A comprehensive investigation of copper pitting corrosion in a drinking water distribution system. *Corrosion Science*, **52** (6): 1927-1938, DOI: 10.1016/j.corsci.2010.02.013.

Nam, N. D., Hung, T. V., Ngan, D. T., Hung, N. L. T., and Hoi, T. K. N., 2016. Film formation in $Y(4NO_2Cin)_3$ compound on 6061 aluminum alloy to protect against corrosion in chloride ion media. *Journal of the Taiwan Institute of Chemical Engineers*, **67**: 495-504, DOI: 10.1016/j.jtice.2016.08.005.

Nam, N. D., Phung, V. D., Thuy, P. T. P., Dao, V. A., Kim, S. H., and Yi, J. S., 2019. Corrosion behaviours of hot-extruded Al-xMg alloys. *Journal of Materials Research and Technology*, **8** (6): 5246-5253, DOI: 10.1016/j.jmrt.2019.08.047.

Natishan, P. M., Yu, S. Y., O'Grady, W. E., and Ramaker, D. E., 2002. X-ray absorption near edge structure and X-ray photo electron spectroscopy studies of chloride in passive oxide films. *Electrochimica Acta*, **47** (19): 3131-3136, DOI: 10.1016/S0013-4686(02)00232-3.

Rudd, W. J., and Scully, J. R., 1980. The function of the repassivation process in the inhibition of pitting corrosion on ahuminium. *Corrosion Science*, **20** (5): 611-631.

Soltis, J., 2015. Passivity breakdown, pit initiation and propagation of pits in metallic materials – Review. *Corrosion Science*, **90**: 5-22, DOI: 10.1016/j.corsci.2014.10.006.

Theivaprakasam, S., Girard, G., Howlett, P., Forsyth, M., Mitra, S., and MacFarlane, D., 2018. Passivation behaviour of aluminium current collector in ionic liquid alkyl carbonate (hybrid) electrolytes. *NPJ Materials Degradation*, **2** (1): 1-9, DOI: 10.1038/s41529-018-0033-6.

Wagner, M. F., 2018. Light-weight aluminum-based alloys – From fundamental science to engineering applications. *Metals*, **8** (4): 260, DOI: 10.3390/met8040260.

Yang, S. H., Zhang, D. C., and Tian, Y. B., 2008. Study on the corrosion of 5083 Al-Mg alloy in different concentrations of NaCl solution. *Science and Engineering of Nonferrous Metals*, **9** (2): 1-5 (in Chinese with English abstract).

Yohai, L., Schreiner, W. H., Vázquez, M., and Valcarce, M. B., 2011. Surface characterization of copper, zinc and brass in contact with tap water inhibited with phosphate ions. *Applied Surface Science*, **257** (23): 10089-10095, DOI: 10.1016/j.apsusc.2011.07.002.

Zaid, B., Saidi, D., Benzaid, A., and Hadji, S., 2008. Effects of pH and chloride concentration on pitting corrosion of AA6061 aluminum alloy. *Corrosion Science*, **50** (7): 1841-1847, DOI: 10.1016/j.corsci.2008.03.006.

Zazi, N., and Chopart, J., 2017. Dissolution of Ag/AgCl reference electrode and deposition of silver onto the surface of 5083 H321 aluminum alloy, during corrosion in 3wt% NaCl solution at rest potential. *Protection of Metals and Physical Chemistry of Surfaces*, **53** (6): 1114-1119, DOI: 10.1134/S2070205117060235.

(Edited by Ji Dechun)